# Absorption Threshold Extended to 1.15 eV Using InGaAs/GaAsP Quantum Wells for Over-50%-efficient Lattice-matched Quad-junction Solar Cells

Kasidit Toprasertpong[1*], Hiromasa Fujii[1], Tomos Thomas[3], Markus Führer[3], Diego Alonso-Álvarez[3], Daniel J. Farrell[2], Kentaroh Watanabe[2], Yoshitaka Okada[2], Nicholas J. Ekins-Daukes[3], Masakazu Sugiyama[1], and Yoshiaki Nakano[1]

[1] Department of Electrical Engineering and Information Systems, the University of Tokyo, Tokyo, Japan
[2] Research Center for Advanced Science and Technology, the University of Tokyo, Tokyo, Japan
[3] Department of Physics, Imperial College London, London, UK

## ABSTRACT

Bandgap engineering of strain-balanced InGaAs/GaAsP multiple quantum wells (MQWs) allows high-quality materials with an absorption edge beyond GaAs to be epitaxially grown in Ge/GaAs-based multijunction solar cells. We demonstrate MQW solar cells with effective bandgaps ranging from 1.31 eV to as low as 1.15 eV. The bandgap-voltage-offset of MQWs is found to be independent of effective bandgaps and superior to a bulk reference by approximately 0.1 V. This implies the merit of high photovoltage as compared with bulk cells with the same bandgap in addition to their widely bandgap-tunable property. Towards the realization of fully lattice-matched quad-junction devices, we demonstrate a 70-period, 1.15-eV bandgap MQW cell as a promising material in 0.66/1.15/1.51/1.99-eV quad-junction cells, whose practical efficiency has a potential to achieve over 50%. With such a large number of MQWs, the reverse-biased external quantum efficiency reaches an average of over 60% in the spectral region corresponding to a 1.15-eV subcell; this is achieved with only a-few-percent drop at short-circuit condition. The device presented here reaches the target open-circuit voltage and over 75% of the current density required for realizing a 1.15-eV subcell in a 50%-efficient quad-junction solar cell. We believe future devices which exploit light-trapping structures and enhanced carrier extraction will be able to reach the desired target.

## KEYWORDS

Quantum well; Strain compensation; Lattice match; Multijunction subcell; Bandgap engineering; III–V semiconductors

## 1. INTRODUCTION

Enhancement of conversion efficiency from solar energy is one key point to realize cost-effective photovoltaic cells. Among several new concepts of solar cells [1], multijunction cells are currently playing an important role in the realization of high energy conversion efficiency [2–3]. By increasing the number of junctions and choosing the appropriate combination of bandgaps, solar spectrum can be efficiently absorbed with less transmission and carrier-relaxation losses [1,3–4], resulting in higher efficiency than the Shockley–Queisser limit of conventional solar cells [5].

One essential issue of multijunction cell is how to deal with a variety of lattice-constants in different materials. Lattice-matching of subcell materials is necessary for monolithic growth of multijunction cells without introducing misfit dislocations [6]. Fully lattice-matched InGaP/(In)GaAs/Ge multijunction cells have achieved 41.6% efficiency [7] and are widely commercialized with high practical production efficiency [8]. Nevertheless, most lattice-matched cells up-to-date are triple-junction [2], and dealing with larger number of junctions is challenging as more lattice-matched materials with different bandgaps are required. Particularly in the Ge/GaAs-based multijunction design, no compound materials constructed from widely employed elements Al, Ga, In, As, P, and Sb possess bandgaps below 1.4 eV while lattice-matching with Ge/GaAs [9]. Wafer-bonding is one successful technique to realize quad-junction and quintuple-junction as reported with notable efficiency of 44.7% under 297 suns [10] and 38.8% under 1 sun [11], respectively. This technique can connect materials with different lattice-constants without creating dislocations in the photovoltaic active region, but comes with trade-offs of ohmic loss, optical loss, and an additional process. Monolithic growth techniques of narrow-gap materials on Ge/GaAs substrates such as dilute nitride semiconductor [12–15] and inverted metamorphic InGaAs [16–18] are alternative approaches to gain cell efficiency and manufacturing throughput. The significant issue of dilute nitride semiconductor is its poor minority carrier lifetimes which dramatically degrade the open-circuit voltage and the carrier collection. Inverted metamorphic structure uses thick buffer layers to confine the misfit dislocations, but it is still suffering from the remaining dislocations which are difficult to be completely avoided [18]. This becomes more prominent in four or more junction cells for which several buffer layers are required [16–17].

InGaAs/GaAsP multiple quantum wells (MQWs) introduce GaAsP which has a small lattice-constant to balance the strain generated during the growth of large-lattice-constant InGaAs on Ge/GaAs before the InGaAs layer reaches its critical

thickness [19–20]. Owing to a strain-compensation technique, effectively lattice-matched MQWs with a total thickness of more than one micrometer can be grown on GaAs with high crystal quality [21] and desirable cell performance [22]. Since their absorption edge is determined by narrow-gap InGaAs, MQWs are promising materials for bandgap combinations below the (In)GaAs bandgap of 1.4 eV in Ge/GaAs-based multijunction cells [20,23].

So far, most research works have been studying InGaAs/GaAsP MQWs with effective bandgaps ranging from 1.20 to 1.35 eV for InGaP/MQW dual-junction and InGaP/MQW/Ge triple-junction applications [22–26]. Triple-junction solar cells with 100-period, 1.34-eV absorption-peak InGaAs/GaAsP MQW midcells have been achieved and efficiency more than 42% was reported [26]. However, as will be discussed in the next session, high-efficiency quad-junction solar cells require materials with effective bandgaps as low as 1.15 eV in spite that MQW cells with these bandgaps have not been reported.

Here, the authors focus on a bandgap combination of 0.66/1.15/1.51/1.99 eV for quad-junction cells with estimated efficiency over 50% and discuss the MQW design to achieve 1.15 eV. Firstly, we investigate MQW solar cells with different effective bandgaps to clarify advantages and issues in using MQWs as subcells. Then, for the first time, we demonstrate 70-period MQW solar cells with 1.15-eV absorption edge, promising output current, and high open-circuit voltage for the realization of fully lattice-matched quad-junction cells.

## 2. SIMULATION AND DESIGN

### 2.1. Bandgap combination and efficiency estimation

Figure 1(a) shows the estimated practical efficiency of series-connected quad-junction cells for a given bandgap combination. The bottom cell is fixed to a Ge substrate and each top-cell bandgap is chosen so that the efficiency reaches maximum for a given Ge/third/second subcell combination. The efficiencies were estimated using 90% external quantum efficiency (EQE), 30% radiative efficiency, and 12.3 $m\Omega \cdot cm^2$ series resistance based on recent high-performance III–V cell parameters [27–28]. In order to achieve efficiency over 50%, the bandgap of the second and third subcell has to be in the range of 1.41-1.51 eV and 1.02-1.15 eV, respectively.

Figure 1(b) shows a roadmap for lattice-matched quad-junction cells towards 50% efficiency. 0.66/1.15/1.51/1.99 eV is a notable bandgap combination since it provides an estimated efficiency of 50.1%. As previously mentioned, realizing lattice-matched 1.15-eV subcells is a challenging material-related issue for this quad-junction

combination, and our approach is to focus on InGaAs/GaAsP MQWs. Although Figure 1(a) suggests that the optimum bandgap of the third subcell should be lower than 1.15 eV, less than 1% efficiency gain after decreasing the third-subcell bandgap from 1.15 eV to the optimum value of 1.04 eV is expected. In addition, we will show in the later sessions that decreasing the effective bandgap of MQWs by only a few hundred meV will cause significant difficulties in crystal growth and carrier collection. Therefore, the 1.15-eV MQW becomes our target to achieve sufficiently high efficiency. The roadmap discussing other approaches and more details on the efficiency estimation can be found in [29].

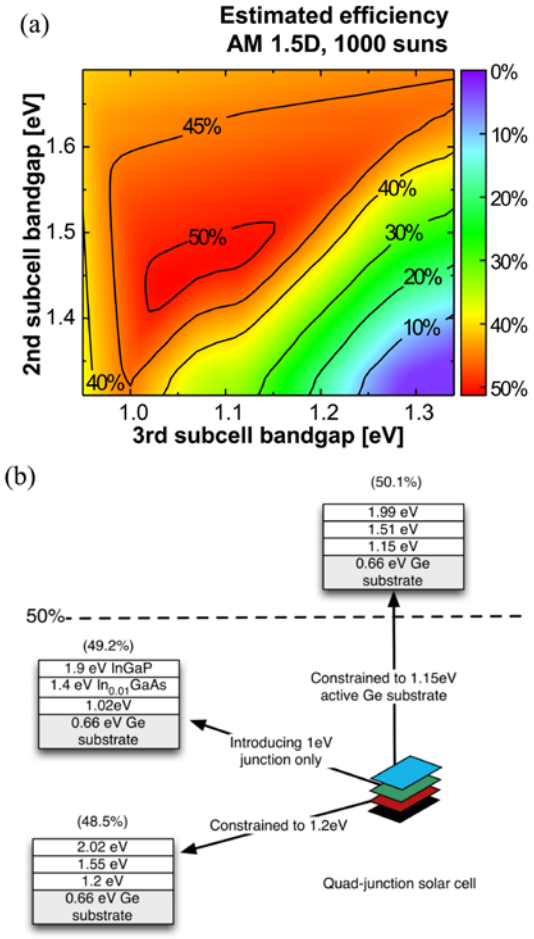


**Figure 1.** Estimated practical efficiencies of series-connected quad-junction solar cells under 1000 suns. (a) Estimated efficiencies as a function of the second and the third subcell bandgaps when the bottom cell is assigned to be Ge. The top-cell bandgap is optimized to give the maximum efficiency. The top cell is treated as the first subcell and the others are numbered in order. (b) Roadmap for lattice-matched quad-junction solar cells towards energy conversion efficiency beyond 50%.

## 2.2. Structure design

MQWs with effective bandgap of 1.15 eV handle high strain per layer and have to be carefully designed. Figure 2 shows the InGaAs thickness required for 1.15 eV. The required thicknesses were calculated using k· p approximation with $GaAs_{0.8}P_{0.2}$ barriers and no interlayers between InGaAs and GaAsP. The effect of strain on the band structures was taken into account through deformation potentials [9,30–31], but the strain effect on other parameters such as effective mass was not included. The simulated effective bandgap tends to be lower than the experimental result when the indium content becomes high; hence we used this simulation only in the qualitative discussion. The Matthews–Blakeslee critical thickness [32] is also plotted together with their ratio. This simulation result indicates that higher indium content is preferred to avoid the well thickness exceeding the critical thickness during the growth of InGaAs layers. Furthermore, the reduction of required InGaAs thickness by introducing high indium content results in higher absorption coefficient in MQWs [22,33]. As the first trial, we implemented indium content as high as 32.5% in InGaAs/GaAsP MQWs.

Moreover, abruptness of atomic content at the interface between InGaAs and GaAsP layers degrades the crystal quality. Inserting interlayers with lattice-constant lying between InGaAs and GaAsP can improve crystal quality, allowing larger number of quantum wells to be grown without lattice relaxation [21–22,34]. This suppresses non-radiative recombination at the heterointerfaces and thus improves the ideality factor [35]. In addition, insertion of interlayers can lower the effective bandgap, extending the absorption edge with thinner InGaAs wells [22]. For this reason, we inserted

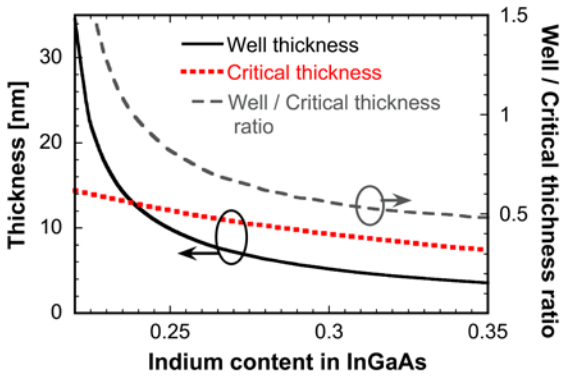


**Figure 2.** InGaAs well thickness required for 1.15 eV and Matthews–Blakeslee critical thickness as a function of indium content. The required thickness was estimated using the k· p method. Ratios of these two thicknesses are shown as a dashed line.

$In_{0.14}Ga_{0.86}As/GaAs/GaAs_{0.85}P_{0.15}$ graded interlayers in between InGaAs and GaAsP in our structures.

Since MQWs with absorption edge at 1.15 eV is comparatively deep, collection of carriers from MQWs becomes critical. GaAsP has wide bandgap and acts as potential barriers in this structure. We need to thin these barriers to facilitate tunneling transport [24,36] or to lower the barriers to utilize thermal escape [37]. The former approach is not easy for these MQWs which have high indium content and wide InGaAs wells because large volume of GaAsP barriers is required for strain-balancing. The latter approach was employed in this work using comparatively low phosphorus composition of 20% in GaAsP. The thickness of GaAsP was adjusted so that the compressive strain from InGaAs is compensated.

## 3. EXPERIMENTAL DETAILS

Samples employed in this work were grown by metal-organic vapor phase epitaxy (MOVPE) on (001) oriented n-GaAs substrates at 100 mbar, 610 °C. Trimethylgallium (TMGa), trimethylindium (TMIn), tertiarybutylarsine (TBAs), tertiarybutylphosphine (TBP), dimethylzinc (DMZn) for p-doping, and hydrogen sulfide ($H_2S$) for n-doping were used as source materials with $H_2$ carrier gas. The schematic of sample structures is shown in Figure 3(left). Each sample began with an n-GaAs buffer layer (100 nm), followed by a $1 \times 10^{17}$ $cm^{-3}$ doped n-type base (400 nm). After growing an i-region, whose details differ in each sample, a $2 \times 10^{18}$ $cm^{-3}$ doped p-type emitter (100 nm), a p-doped $In_{0.47}Ga_{0.53}P$ window layer (25 nm), and a p-contact layer (50 nm) were grown. In different cells, only structures in i-region were changed. In Session 4.1, the V/III ratio for i-region growth was approximately 10 to 15, depending on the layer, and the growth rate was 13 nm/min. The V/III ratio and the rate of i-region growth were changed to 45-60 and 6 nm/min, respectively, in the later sessions in an attempt to improve the crystal quality. AuGe (350 nm) annealed with Ni (20 nm) at 380°C for 2.5 minutes, and Ti (20 nm)/Au (300 nm) were used as ohmic contacts at n-side and p-side, respectively. ZnS (53 nm)/$SiO_2$ (107 nm) antireflection coating (ARC) was applied to some samples.

Atomic contents and layer thicknesses were confirmed by X-ray diffraction measurement. Effective bandgaps were estimated by both photoluminescence peaks using a 532-nm, 40-μW laser, and lowest-energy absorption peaks using Fourier transform infrared spectroscopy, which are well agreed with each other. The values are higher than the estimation focusing on cut-off energies in absorption spectra by approximately 0.01 eV. EQE was measured by monochromatic illumination with 2.5 $mW/cm^2$ intensity, 20-nm spectral resolution under AM1.5G one-sun light bias.

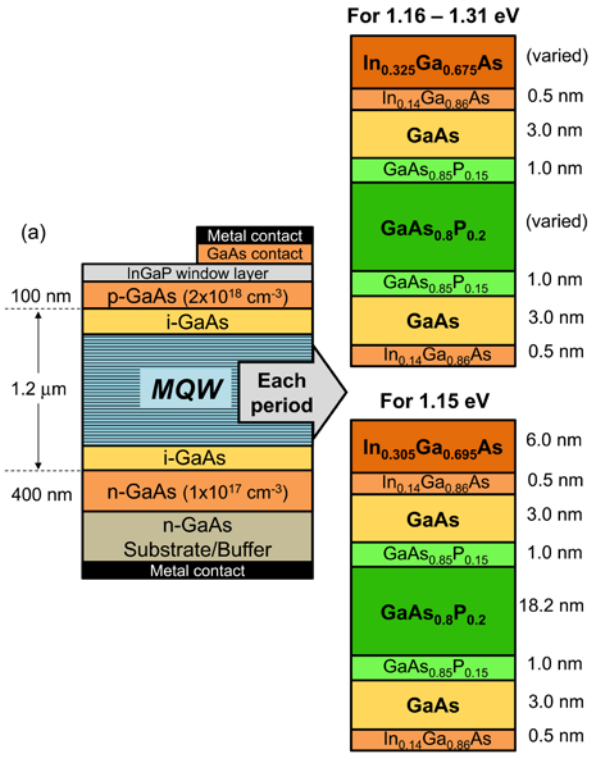


**Figure 3.** Cell structures of MQW solar cells. The structure on the right is the details of stacked layers in each period of MQWs. 35 periods of MQWs were stacked for a wide range of effective bandgaps, and 70 periods were stacked in the last 1.15-eV MQW cell.

## 4. RESULTS AND DISCUSSION

### 4.1. MQW with various effective bandgaps

Five samples were investigated with 1.2 μm-thick i-regions containing 35-period MQWs with various effective bandgaps in the middle of the regions. The i-region thickness of 1.2 μm is small enough to guarantee that the i-region with net background carrier concentration of the order of $10^{14}$ $cm^{-3}$, controlled with an appropriate amount of sulfur donors by the method in [38], is entirely depleted. The MQW structure is shown in Figure 3(top-right). To systematically investigate the bandgap dependency, The thicknesses of $In_{0.325}Ga_{0.675}As$ wells and $GaAs_{0.8}P_{0.2}$ barriers were varied from 1.5, 2.3, 3.2, 4.3 to 5.2 nm and from 5.1, 7.6, 10.6, 14.3 to 17.3 nm, respectively, with the target effective bandgap of 1.15 eV in the thickest MQW. The phosphorous content in $GaAs_{0.8}P_{0.2}$ is constant, so the height of potential barriers is the same and a fair comparison on the effect of well depth can be made. $In_{0.14}Ga_{0.86}As$ (0.5 nm)/GaAs (3.0 nm)/$GaAs_{0.85}P_{0.15}$ (1.0 nm) graded interlayers was fixed. No ARC was applied at this

stage.

Figure 4 shows the measured effective bandgaps of MQW samples. The effective bandgaps decreases from 1.31, 1.25, 1.21, 1.17 to 1.16 eV as the well thickness increases. The corresponding absorption peak wavelengths are 949, 990, 1028, 1063, and 1068 nm, respectively. The bandgap of the thickest-well device does not follow the trend of the others due to the crystal quality issue as will be discussed in the next sub-session. Figure 5 shows the cell properties for all the five devices. In this sub-session, the thickest-well device is excluded and only other four MQW cells are considered in the discussion.

Since there is no ARC in these cells, reflectance is high and internal quantum efficiency (IQE) was considered. IQE results are shown in Figure 5(a)-(b). The aperture areas, excluding the shadow loss, were used in the calculation. Current generated by illumination wavelength beyond GaAs absorption edge is from the absorption in MQWs. The peak IQE value at the 1e-1hh transition, the lowest-energy peak in IQE spectra, is found to have weak dependency on effective bandgap, indicating that the absorption per well per optical transition is almost constant despite 3-4 times the difference in well thickness. The result agrees well with that obtained from Fermi's Golden Rule, which indicates that the absorption per well does not explicitly depend on the thickness [33].

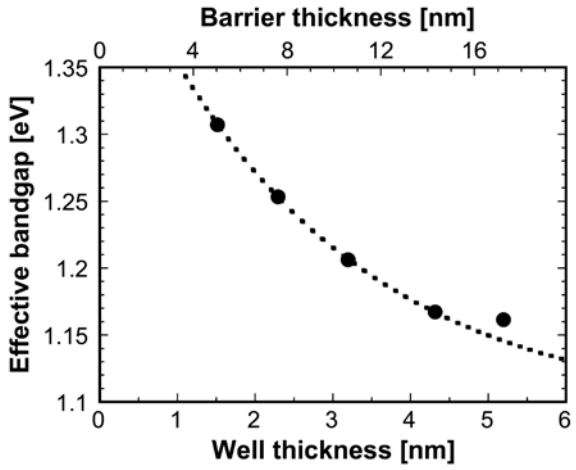


**Figure 4.** Measured effective bandgap of MQWs as a function of InGaAs well thickness. Corresponding barrier thickness is indicated in the top x-axis. Thickness shown on the axis does not include the thickness of interlayers. The trend is shown as a dot line. The last data point does not follow the trend due to poor crystal quality.

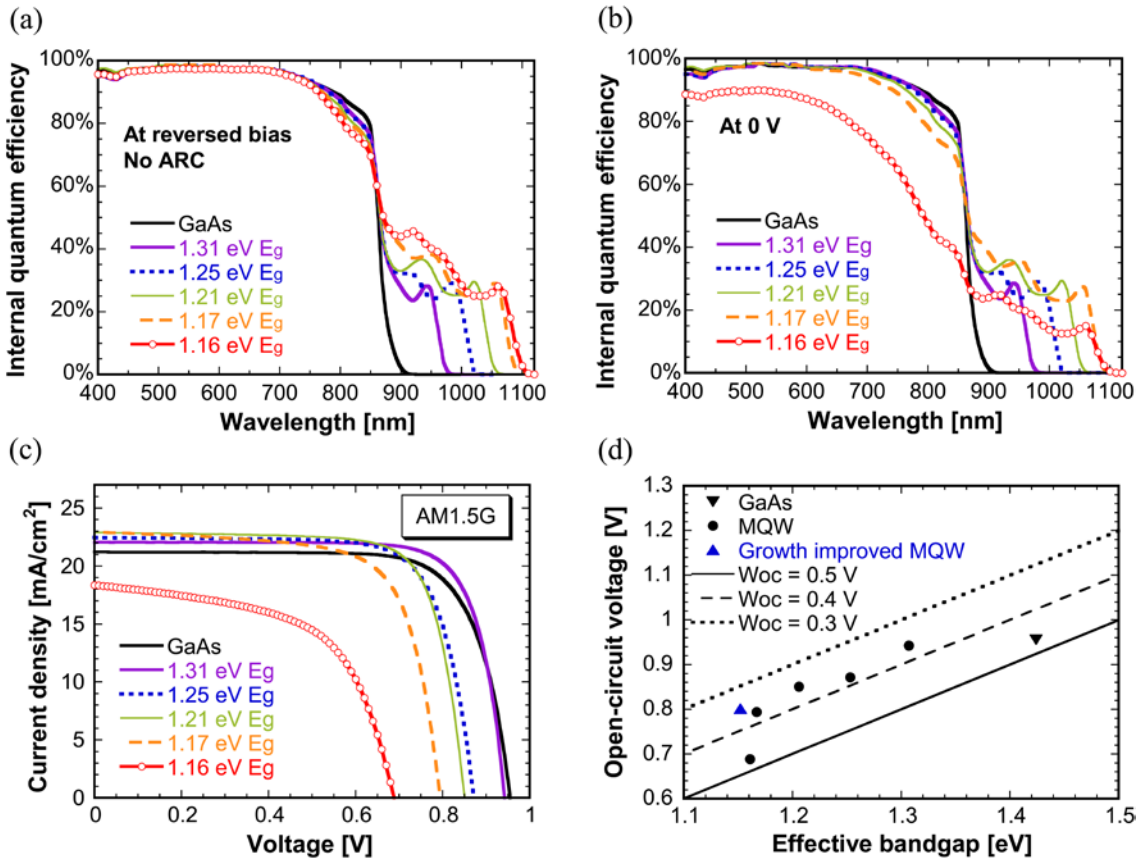


**Figure 5.** Cell performance of GaAs reference and 35-period MQW solar cells having different effective bandgaps under AM1.5G, 1 sun. The aperture areas were used in the calculation. IQE under (a) sufficient reverse bias (-6 V for 1.16-eV MQW, -3.5 V for 1.17-eV MQW, -2 V for others) and under (b) short-circuit condition. (c) *J–V* characteristics. (d) Open-circuit voltage. Three straight lines indicate constant bandgap-voltage-offset $W_{oc}$ of 0.3, 0.4 and 0.5 V. Averaged $W_{oc}$ of 0.36 V is obtained from MQW cells.

This suggests that for a given effective bandgap, a new design with thinner wells, if possible, is reasonable for a further approach to reduce the amount of required materials. One example for this kind of design is high-aspect ratio structures introduced in [25]. Up to the third optical transition has been observed. This enhances IQE at the high-energy region of MQW absorption in narrow-gap MQW cells. Small drop of IQE near 800 nm as the effective bandgap decreases is due to the increasing total thickness of $GaAs_{0.8}P_{0.2}$ strain-compensation layer, which has wider bandgap than GaAs, approximately 1.63 eV, and thus cannot absorb light in this region.

The extension of IQE in narrow-gap MQWs increases the output current as shown

in Figure 5(c). However, a drop in IQE, and so as in output current, at $V \geq 0$ from the values at reverse bias becomes remarkable and degrades the fill factor (*FF*) from 75% in the GaAs reference cell to 69% in the 1.17-eV MQW cell as the effective bandgap becomes narrower. This is the result from either or both of more difficult thermal escape of photoexcited carriers from deeper quantum wells and lower crystal quality due to larger strain in wider wells. Under reverse bias, the internal electric field becomes strong and most of photoexcited carriers can be collected regardless of transport obstruction [39]. Therefore, IQE under reverse bias is not affected by the carrier transport issue, as can be confirmed by the good agreement of IQE values in the 400-700 nm region.

Figure 5(d) shows the open-circuit voltage as a function of effective bandgap. We investigate bandgap-voltage-offset $W_{oc} = E_g/q - V_{oc}$ in the MQW and the bulk reference cells. $E_g$ in the $W_{oc}$ calculation represents the absorption threshold energy, which is the bandgap for bulk cells and the effective bandgap for MQW cells. Since the base thickness, the emitter thickness, and the metal contact pattern have not been optimized enough, $W_{oc}$ of the GaAs reference cell under 1 sun is 0.47 V, which is relatively higher than the high-performance cells whose $W_{oc}$ is 0.4 V in average [40]. In spite of the high $W_{oc}$ of the bulk reference, on the other hand, $W_{oc}$ of the MQW solar cells are comparatively low at $0.36 \pm 0.01$ V, lower than the common bulk cells in [40] and superior than the reference by approximately 0.1 V. This finding suggests that MQW solar cells tend to have significantly higher voltage than bulk solar cells having the same bandgap. The superior $W_{oc}$ in MQWs has also been reported in other MQW materials, such as AlGaAs/GaAs, InGaP/GaAs, and InP/InGaAs, confirming the generality of this property even though the reason is still under investigation [41]. This is, in addition to the capability to extend absorption threshold from GaAs while keeping lattice-match, one outstanding advantage of MQWs which encourages them to be high-potential candidates in the realization of lattice-matched multijunction solar cells.

### 4.2. Growth improvement

It is obvious from the effective bandgap disagreeing with the trend in Figure 5 that crystal degradation in a sample with deep, thick wells hinders MQW from achieving low bandgap. The degradation in cell performance can be found in drops in IQE (Figure 5(b)), short-circuit current $J_{sc}$ (Figure 5(c)), and $V_{oc}$ (Figure 5(d)) from the trends they should have followed. Moreover, as shown in Figure 6(a), we have found that the dark current density dramatically increases in the degraded MQW cell. This large dark current is the main attribution of the severe degradation in $V_{oc}$. The high dark current

density with the ideality factor of 2 indicates that there are a lot of defects in the i-region which promote the non-radiative recombination. The remarkable non-radiative process significantly degrades the carrier collection efficiency under forward bias in addition to the difficult thermal escape in deep wells. IQE recovery under reverse bias (Figure 5(a)) confirms that the promising cell performance can be achieved by improving the crystal quality.

Figure 6(b) shows the surface image of this 5.2-nm-$In_{0.325}Ga_{0.675}As$ MQW cell. Some 3D islands were found on the sample surface. This phenomenon has been reported that indium content higher than 0.3 let indium aggregate easily due to high surface mobility of indium adatoms, allowing it to be more stable to form islands via the 3D growth mode [42–44]. Furthermore, the aggregation is enhanced by the strain during the growth [45].

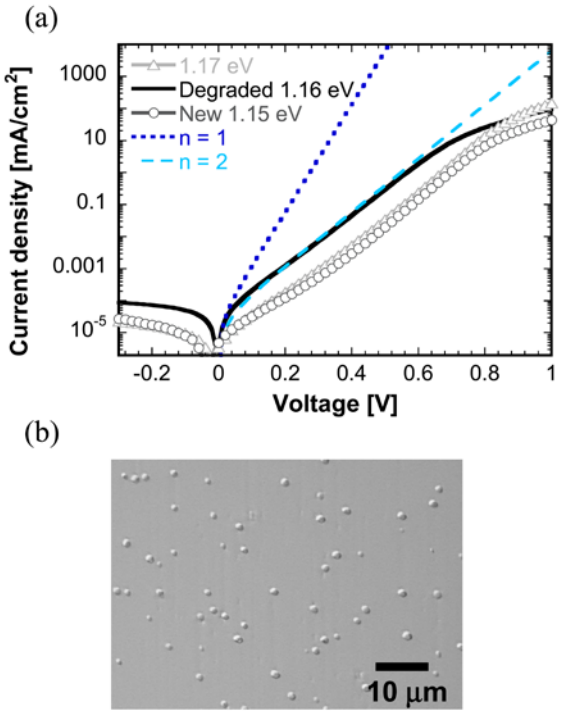


**Figure 6.** Degraded crystal quality and cell performance in the 1.16-eV MQW with 5.2 nm-thick $In_{0.325}Ga_{0.675}As$ wells. (a) Dark *J–V* characteristic. The dark current density of the 1.17-eV MQW cell, which does not experience the performance degradation as severely as the 1.16-eV cell, is shown as an open-triangle line for comparison. A line with open circles is the performance of the MQW cell after growth improvement. Two straight lines indicate the ideality factor of 1 and 2. (b) Differential interference microscope image of the layer surface.

We decreased the indium content of InGaAs to 30.5% to reduce the indium segregation. During the growth of the MQW region, the V/III ratio was increased to 45-60 and the growth rate was reduced to 6 nm/min as are suggested in [43–44] that these will help suppress the segregation. The final structure was 35-period MQW consisting of $In_{0.305}Ga_{0.695}As$ (6.0 nm) as a well layer and $GaAs_{0.8}P_{0.2}$ (18.2 nm) as a barrier layer (Figure 3(bottom-right)). As a result, the effective bandgap of 1.15 eV has been successfully achieved in this structure. The dark current density improved by one order of magnitude is shown as the open-circle line in Figure 6(a) and the open-circuit voltage is shown as an upright triangle in Figure 5(d). $W_{oc}$ of 0.35 V has been obtained, suggesting that the crystal degradation is sufficiently suppressed in the new structure. Nevertheless, we found later that decreasing the indium content is the main factor for this success by confirming that growth of 6.0-nm-$In_{0.305}Ga_{0.695}As$-MQWs was still successful with the previous V/III ratio and growth rate.

### 4.3. 1.15-eV bandgap MQW cell performance

Other than the 35-period cell, a 70-period, 1.15-eV MQW cell was prepared by the same growth procedure. As 1.2 μm is not enough for 70 periods, the i-region only in the latter cell was extended to 2.4 μm. ARC was applied to these solar cells and the GaAs reference cell to investigate the maximum performance it can be achieved. Note that the reference cell was the same sample as used in the last sub-session, thus the i-region thickness was 1.2 μm.

EQE spectra of these solar cells are shown in Figure 7(a)-(b) for reverse-bias and short-circuit conditions. The aperture areas were used in the calculation. Under reverse bias, the EQE peaks at 1.15 eV in 35- and 70-period MQWs are found to be 29% and 46%, respectively. Our measurement system has a tendency to underestimate peak EQEs since the spectral resolution is 20-nm wide, so the actual peak EQEs are thought to be higher than these measured values. The averaged EQE values in the 1.15-1.51 eV range corresponding to the subcell absorption are 43% and 62%, respectively, which are remarkable considering that no light-trapping structures were implemented while most absorption in this range comes from MQWs (The averaged EQE for the reference in the same range is 16%). The higher EQE than the reference cell at 800 nm is owing to the thicker i-region.

It is plausible to attribute the EQE drop under $V \geq 0$ to the degraded thermal escape from deep quantum wells rather than poor crystal quality since the acceptable dark current and high short-circuit EQE at MQW absorption wavelength have been obtained. The difficulty in carrier escape from deep wells was exacerbated by the thicker i-region

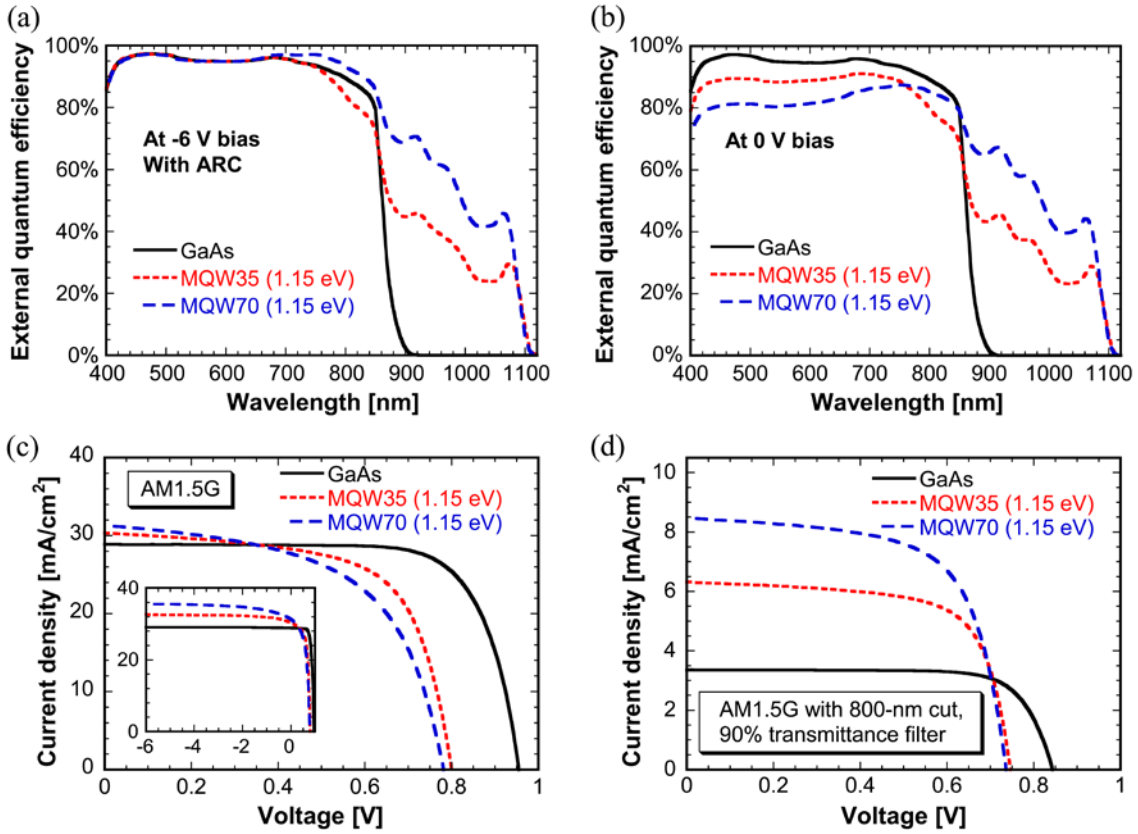


**Figure 7.** Solar cell performance of 35-period and 70-period, 1.15-eV MQW cells with antireflection coating layers. The performance of a GaAs reference cell whose i-region thickness is equal to the 35-period cell but is a half of the 70-period cell is also shown. The aperture areas were used in the calculation. EQE under (a) -6 V reverse bias, and (b) short-circuit condition. *J–V* characteristics under (c) 1-sun AM1.5G, with an inset showing the curves extended to the reverse bias region, and (d) 1-sun AM1.5G filtered by a 800-nm cut, 90% transmittance filter (FEL0800, Thorlabs).

in the 70-period MQW cell, decreasing the built-in field, possibly making the background-doped i-region partly undepleted, and consequently further reducing short-circuit EQE. EQE under reverse bias in Figure 7(a) is a good estimation for the maximum short-circuit EQE that would be obtained if the structure was optimized for efficient carrier collection.

Figure 7(c) shows the *J–V* characteristics under AM1.5G, 1 sun. As shown in the inset, the maximum current has been significantly enhanced from 29.1 to 35.6 mA/cm$^2$ after inserting the 70-period, 1.15-eV MQW structure. In contrast, the increment of $J_{sc}$ is found not to be as high as expected due to degraded carrier collection. $V_{oc}$ of the

70-period cell is found to be 0.78 V, lower than that of 35-period cell (0.80 V) by 0.02 V. This is the effect of degraded carrier collection which reduces the photocurrent

$$J_{photo} = J_{illu} - J_{dark} \quad (1)$$

where $J_{illu}$ and $J_{dark}$ are the output current with and without illumination, respectively. We estimate that the $V_{oc}$ of the 70-period cell can recover to 0.81 V by assuming the same collection percentage of photocurrent as the 35-period cell, indicating that the remarkable $W_{oc}$ of MQW solar cells preserves with increasing number of quantum-well stacks if the carrier-collection efficiency is not degraded.

To approximately simulate the cell performance as 1.15-eV subcells inserted in 0.66/1.15/1.51/1.99-eV quad-junction cells, AM1.5G was filtered by a 800-nm cut, 90% transmittance filter (FEL0800, Thorlabs). The *J–V* characteristics are shown in Figure 7(d) and the cell parameters are summarized in Table I. This filter can acceptably mimic the solar spectrum reaching the third subcell as can be seen in good agreement between the photocurrent under filtered illumination and the integrated EQE.

**Table I.** Cell performance parameters as the 1.15-eV third subcells under filtered 1 sun illumination

| Cell | $J_{reverse}$ [mA/cm2][1] | | $J_{sc}$ [mA/cm2] | | $V_{oc}$ [V] | $FF$ [%] | $\eta$ [%][4] | |
|---|---|---|---|---|---|---|---|---|
| | 800-nm filter[2] | From EQE[3] | 800-nm filter[2] | From EQE[3] | | | $\eta_{filter}$ | $\eta_{sub}$ |
| GaAs ref. | 3.4 | 2.6 | 3.4 | 2.5 | 0.844 | 76.0 | 6.1 | 12.0 |
| 35-period | 6.8 | 6.3 | 6.3 | 6.0 | 0.746 | 68.4 | 9.0 | 17.7 |
| 70-period | 9.2 | 8.9 | 8.5 | 8.3 | 0.736 | 65.0 | 11.3 | 22.3 |
| Target[5] | 11.6 | | | | 0.74 | 77.0 | 18.4 | 36.3 |

[1]Current density under -6 V reverse bias

[2]Current density under AM1.5G illumination filtered by a 800-nm cut, 90% transmittance filter (FEL0800, Thorlabs)

[3]Current density calculated by integrating EQE spectra from 1.51 eV (820 nm) to the low energy part

[4]$\eta_{filter}$ and $\eta_{sub}$ are the efficiencies calculated by assuming the incident energy of 35.9 mW/cm$^2$ (AM1.5G with a FEL0800 filter) and 18.2 mW/cm$^2$ (AM1.5G with a FEL0800 filter excluding photon energies lower than 1.15 eV), respectively.

[5]Simulated 1-sun parameters of the 1.15-eV subcell in the 50.1%-efficient (1000 suns) quad-junction cell shown in Figure 1(b)

The simulated 1-sun performance of the 1.15-eV subcell in the 0.66/1.15/1.51/1.99-eV quad-junction cell having the target efficiency of 50.1% at 1000 suns (Figure 1(b)) is indicated in the last row of Table I. Over three fourths of 11.6 mA/cm$^2$, the photocurrent required for 50% efficiency, has been achieved under reverse bias. The target current can be approached by introducing a distributed Bragg reflector, which has been reported in other works showing that it can enhance EQE of MQWs from 42% to 70% [46]. The needed optical path length enhancement is estimated to be a feasible value of 1.8 times.

Owing to the excellent $W_{oc}$ in MQW cells, the target $V_{oc}$ of 0.74 V has been achieved under filtered 1 sun regardless of low *FF*. Further improvement in *FF* as well as $V_{oc}$ is expected if we can design MQW structures from which photogenerated carriers can be efficiently extracted out. By assuming perfect carrier collection—no drop in photocurrent $J_{photo}$—at forward bias, we could get FF of 76%, close to the target *FF*, and $V_{oc}$ of 0.77 V, surpassing the target value in both 35- and 70-period MQW cells. The high voltage and promising photocurrent suggest the feasibility of 1.15-eV bandgap MQW solar cells to realize fully lattice-matched quad-junction solar cells with the target efficiency of 50%.

## 5. CONCLUSIONS

We have investigated 1.15-eV bandgap, strain-balanced InGaAs/GaAsP MQWs as promising narrow-gap materials towards high-efficiency, fully lattice-matched quad-junction solar cells on Ge/GaAs substrates. In addition to their capability to extend the absorption threshold to the challenging narrow-gap region, InGaAs/GaAsP MQW solar cells are found to have significantly superior bandgap-voltage-offset than bulk cells, lower than the GaAs reference cell by 0.1 V. Using the design of optimized atomic contents of ternary alloys and insertion of graded interlayers, 1.15-eV MQW solar cells have been demonstrated for the first time with the $In_{0.305}Ga_{0.695}As$ (6.0 nm)/interlayer/$GaAs_{0.8}P_{0.2}$ (18.2 nm) MQW structure. Finally, we have studied that cell performance as a subcell in the 0.66/1.15/1.51/1.99-eV quad-junction configuration, whose cell efficiency is estimated to be over 50%. A 70-period, 1.15-eV MQW solar cell shows reverse-biased external quantum efficiency of 62% averaged in the 1.15-1.51-eV spectrum range and more than 45% at the 1.15-eV absorption peak. After filtering AM1.5G corresponding to the absorption by the overlying cells, it generates current density of 9 mA/cm$^2$, which is more than 75% of current in the target quad-junction cell, and successfully achieves the $V_{oc}$ of the target value. Approaches using (1) light-trapping structures to increase the absorption, (2) MQW design

improvement to enhance carrier transport, and (3) further study on the performance when inserting MQWs in the n-on-p structure under high sunlight concentration would lead to the realization of lattice-matched 0.66/1.15/1.51/1.99-eV quad-junction solar cells towards 50% efficiency.


## ACKNOWLEDGEMENTS

A part of this study is supported by the Research and Development of Innovative Solar Cell program, New Energy and Industrial Technology Development Organization (NEDO), Japan and EU-Japan Coordinated Project "A new generation of concentrator photovoltaic cells, modules and systems".


## REFERENCES


1. Green MA. Third generation photovoltaics: ultra-high conversion efficiency at low cost. *Progress in Photovoltaics: Research and Applications* 2001; **9**: 123–135.
2. Green MA, Emery K, Hishikawa Y, Warta W, Dunlop ED. Solar cell efficiency tables (version 44). *Progress in Photovoltaics: Research and Applications* 2014; **22**: 701–710.
3. King RR, Bhusari D, Larrabee D, Liu XQ, Rehder E, Edmondson K, Cotal H, Jones RK, Ermer JH, Fetzer CM, Law DC, Karam NH. Solar cell generations over 40% efficiency. *Progress in Photovoltaics: Research and Applications* 2012; **20**: 801–815.
4. Brown AS, Green MA. Detailed balance limit for the series constrained two terminal tandem solar cell. *Physica E: Low-dimensional Systems and Nanostructures* 2002; **14**: 96–100.
5. Shockley W, Queisser HJ. Detailed balance limit of efficiency of pn junction solar cells. *Journal of Applied Physics* 1961; **32**: 510–519.
6. Takamoto T, Kaneiwa M, Imaizumi M, Yamaguchi M. InGaP/GaAs-based multijunction solar cells. *Progress in Photovoltaics: Research and Applications* 2005; **13**: 495–511.
7. King RR, Boca A, Hong W, Liu XQ, Bhusari D, Larrabee D, Edmondson KM, Law DC, Fetzer CM, Mesropian S, Karam NH. Bandgap engineering architectures for high efficiency multijunction concentrator cells. *Proceedings of the 24th European Photovoltaic Solar Energy Conference*, Hamburg, Germany, 2009; 55–61.
8. Ermer JH, Jones RK, Hebert P, Pien P, King RR, Bhusari D, Brandt R, Al-Taher O, Fetzer C, Kinsey GS, Karam N. Status of C3MJ+ and C4MJ production concentrator solar cells at Spectrolab. *IEEE Journal of Photovoltaics* 2012; **2**: 209–213.
9. Vurgaftman I, Meyer JR, Ram-Mohan LR. Band parameters for III–V compound semiconductors and their alloys. *Journal of Applied Physics* 2001; **89**: 8515–8575.
10. Dimroth F, Grave M, Beutel P, Fiedeler U, Karcher C, Tibbits TND, Oliva E, Siefer G, Schachtner M, Wekkeli A, Bett AW, Krause R, Piccin M, Blanc N, Drazek C, Guiot E, Ghyselen B, Salvetat T, Tauzin A, Signamarcheix T, Dobrich A, Hannappel T, Schwarzburg K. Wafer bonded four-junction GaInP/GaAs//GaInAsP/GaInAs concentrator solar cells with 44.7% efficiency. *Progress in Photovoltaics: Research and Applications* 2014; **22**: 277–282.

11. Chiu PT, Law DC, Woo RL, Singer SB, Bhusari D, Hong WD, Zakaria A, Boisvert J, Mesropian S, King RR, Karam NH. 35.8% space and 38.8% terrestrial 5J direct bonded cells. *40th IEEE Photovoltaic Specialist Conference*, Denver, CO, USA, 2014.
12. Friedman DJ, Geisz JF, Kurtz SR, Olson JM. 1-eV solar cells with GaInNAs active layer. *Journal of Crystal Growth* 1998; **195**: 409–415.
13. Jackrel DB, Bank SR, Yuen HB, Wistey MA, Harris JS, Ptak AJ, Johnston SW, Friedman DJ, Kurtz SR. Dilute nitride GaInNAs and GaInNAsSb solar cells by molecular beam epitaxy. *Journal of Crystal Growth* 2011; **335**: 66–69.
14. Miyashita N, Ahsan N, Islam MM, Okada Y. Study on the Device Structure of GaInNAs (Sb) based solar cells for use in 4-junction tandem solar cells. *Proceedings of the 38th IEEE Photovoltaic Specialist Conference*, Austin, TX, USA, 2012; 000954–000956.
15. Thomas T, Führer M, Alonso-Álvarez D, Ekins-Daukes NJ, Tan KH, Wicaksono S, Loke WK, Yoon SF, Johnson A. GaNAsSb 1-eV solar cells for use in lattice-matched multi-junction architectures. *40th IEEE Photovoltaic Specialist Conference*, Denver, CO, USA, 2014.
16. Law DC, Liu WQ, Boisvert JC, Redher EM, Fetzer CM, Mesropian S, King RR, Edmondson KM, Jun B, Woo RL, Krut DD, Chiu PT, Bhusari DM, Sharma SK, Karam NH. Recent Progress of Spectrolab High-Efficiency Space Solar Cells. *Proceeding of the 38th IEEE Photovoltaic Specialist Conference*, Austin, TX, USA, 2012; 003146–003149.
17. Miller N, Patel P, Struempel C, Kerestes C, Aiken D, Sharps P. Terrestrial concentrator four-junction inverted metamorphic solar cells with efficiency > 45%. *40th IEEE Photovoltaic Specialist Conference*, Denver, CO, USA, 2014.
18. Guter W, Schöne J, Philipps SP, Steiner M, Siefer G, Wekkeli A, Welser E, Oliva W, Bett AW, Dimroth F. Current-matched triple-junction solar cell reaching 41.1% conversion efficiency under concentrated sunlight. *Applied Physics Letters* 2009; **94**: 223504-10223504-3, 2009.
19. Bedair SM, Katsuyama T, Chiang PK, El-Masry NA, Tischler M, Timmons M. GaAsP-GaInAsSb Superlattices: a new structure for electronic devices. *Journal of Crystal Growth* 1984; **68**: 477–482.
20. Ekins-Daukes NJ, Barnes JM, Barnham KWJ, Connolly JP, Mazzer M, Clark JC, Grey R, Hill G, Pate MA, Roberts JS. Strained and strain-balanced quantum well devices for high-efficiency tandem solar cells. *Solar Energy Materials & Solar Cells* 2001; **68**: 71–87.
21. Fujii H, Wang Y, Watanabe K, Sugiyama M, Nakano **Y**. Suppressed lattice relaxation during InGaAs/GaAsP MQW growth with InGaAs and GaAs ultra-thin interlayers. *Journal of Crystal Growth* 2012; **352**: 239–244.
22. Fujii H, Toprasertpong K, Wang Y, Watanabe K, Sugiyama M, Nakano Y. 100-period, 1.23-eV bandgap InGaAs/GaAsP quantum wells for high-efficiency GaAs solar cells: toward current-matched Ge-based tandem cells. *Progress in Photovoltaics: Research and Applications* 2014; 22: 784–795
23. Adams JGJ, Browne BC, Ballard IM, Connolly JP, Chan NLA, Ioannides A, Elder W, Stavrinou PN, Barnham KWJ, Ekins-Daukes NJ. Recent results for single-junction and tandem quantum well solar cells. *Progress in Photovoltaics: Research and Applications* 2011; **19**: 865–877.

24. Wang Y, Wen Y, Sodabanlu H, Watanabe K, Sugiyama M, Nakano Y. A superlattice solar cell with enhanced short-circuit current and minimized drop in open-circuit voltage. *IEEE Journal of Photovoltaics* 2012; **2**: 387–392.
25. Fujii H, Wang Y, Watanabe K, Sugiyama M, Nakano Y. High-aspect ratio structures for efficient light absorption and carrier transport in InGaAs/GaAsP multiple quantum well solar cells. *IEEE Journal of Photovoltaics* 2013; **3**: 859–867.
26. Browne B, Lacey J, Tibbits T, Bacchin G, Wu TC, Liu JQ, Chen X, Rees V, Tsai J, Werthen JG. Triple-Junction Quantum-Well Solar Cells in Commercial Production. *AIP Conference Proceedings* in *9th International Conference on Concentrator Photovoltaic Systems*, Miyazaki, Japan, 2013; **1556**: 3–5.
27. Chan NLA, Ekins-Daukes NJ, Adams JGJ, Lumb MP, Gonzalez M, Jenkins PP, Vurgaftman I, Meyer JR, Walters RJ. Optimal bandgap combinations—does material quality matter? *IEEE Journal of Photovoltaics* 2012; **2**: 202–208.
28. Nishioka K, Takamoto T, Agui T, Kaneiwa M, Uraoka Y, Fuyuki T. Evaluation of InGaP/InGaAs/Ge triple-junction solar cell and optimization of solar cell's structure focusing on series resistance for high-efficiency concentrator photovoltaic systems. *Solar Energy Materials & Solar Cells* 2006; **90**: 1308–1321.
29. Thomas T, Wilson T, Führer M, Alonso-Álvarez D, Ekins-Daukes NJ, Lackner D, Kailuweit P, Philipps SP, Bett AW, Toprasertpong K, Sugiyama M, Okada Y. Potential for reaching 50% power conversion efficiency using quantum heterostructures. *Technical Digest of the 6th World Conference on Photovoltaic Energy Conversion*, Kyoto, Japan, 2014.
30. Kuo CP, Vong SK, Cohen RM, Stringfellow GB. Effect of mismatch strain on band gap in IIIV semiconductors. *Journal of Applied Physics* 1985; **57**: 5428–5432.
31. Van de Walle CG. Band lineups and deformation potentials in the model-solid theory. *Physical Review B* 1989; **39**: 1871–1883.
32. Matthews JW, Blakeslee AE. Defects in epitaxial multilayers: I. Misfit dislocations. *Journal of Crystal Growth* 1974; **27**: 118–125.
33. Harrison P. Quantum Wells, Wires and Dots, 3rd edition. Wiley: England, 2009;355–360.
34. Wen Y, Wang Y, Watanabe K, Sugiyama M, Nakano Y. Effect of GaAs step layer thickness in InGaAs/GaAsP stepped quantum-well solar cell. *IEEE Journal of Photovoltaics* 2013; **3**: 289–294.
35. Okada Y, Seki S, Takeda T, Kawabe M. Control of dark currents in multi-quantum well solar cells fabricated by atomic H-assisted molecular beam epitaxy. *Journal of Crystal Growth* 2002; **237–239**: 1515–1518.
36. Toprasertpong K, Fujii H, Wang Y, Watanabe K, Sugiyama M, Nakano Y. Carrier escape time and temperature-dependent carrier collection efficiency of tunneling-enhanced multiple quantum well solar cells. *IEEE Journal of Photovoltaics* 2014; **4**: 607–613.
37. Schneider H, Klitzing Kv. Thermionic emission and Gaussian transport of holes in a GaAs/$Al_xGa_{1-x}As$ multiple-quantum-well structure. *Physical Review B: Condensed Matter and Materials Physics* 1988; **38**: 6160–6165.
38. Fujii H, Wang Y, Watanabe K, Sugiyama M, Nakano Y., Compensation doping in InGaAs / GaAsP multiple quantum well solar cells for efficient carrier transport and improved cell performance. *Journal of Applied Physics* 2013; **114**: 103101-1–103101-7.

39. Fujii H, Toprasertpong K, Watanabe K, Sugiyama M, Nakano Y. Evaluation of carrier collection efficiency in multiple quantum well solar cells. *IEEE Journal of Photovoltaics* 2014; **4**: 237–243.
40. King RR, Bhusari D, Boca A, Larrabee D, Liu XQ, Hong W, Fetzer CM, Law DC, Karam NH. Band gap-voltage offset and energy production in next-generation multijunction solar cells. *Progress in Photovoltaics: Research and Applications* 2011; **19**: 797–812.
41. Barnham K, Connolly J, Griffin P, Haarpaintner G, Nelson J, Tsui E, Zachariou A, Osborne J, Button C, Hill G, Hopkinson M, Pate M, Roberts J, Foxon T. Voltage enhancement in quantum well solar cells. *Journal of Applied Physics* 1996; **80**: 1201**–**1206.
42. Berger PR, Chang K, Bhattacharya P, Singh J, Bajaj KK. Role of strain and growth conditions on the growth front profile of $In_xGa_{1-x}As$ on GaAs during the pseudomorphic growth regime. *Applied Physics Letters* 1988; **53**: 684–686.
43. Tan HH, Lever P, Jagadish C. Growth of highly strained InGaAs quantum wells on GaAs substrates—effect of growth rate. *Journal of Crystal Growth* 2005; **274**: 85–89.
44. Cederberg JG. Self-assembled quantum dot formation during the growth of $In_{0.4}Ga_{0.6}As$ on GaAs(0 0 1) by metal-organic vapor phase epitaxy: The role of In segregation. *Journal of Crystal Growth* 2007; **307**: 44–50.
45. Ohtake A, Ozeki M, Terauchi M, Sato F, Tanaka M. Strain-induced surface segregation in $In_{0.5}Ga_{0.5}As$/GaAs heteroepitaxy. *Applied Physics Letters* 2002; **80**: 3931–3933.
46. Johnson DC, Ballard I, Barnham KWJ, Bishnell DB, Connolly JP, Lynch MC, Tibbits TND, Ekins-Daukes NJ, Mazzer M, Airey R, Hill G, Roberts JS. Advances in Bragg stack quantum well solar cells. *Solar Energy Materials & Solar Cells* 2005; **87**: 169–179.